Surface brightness comparison of PACS blue array with IRAS and Spitzer/MIPS images

Babar Ali, NHSC

Document change record		
Version	Date	Changes
1.01	12-April-2011	Version 1.01 for public release.

Abstract

This note summarizes results when the observed surface brightnesses from PACS are compared to earlier measurements done by IRAS and Spitzer/MIPS instruments for 4 fields. The comparison is done on a pixel-to-pixel basis by converting, convolving and regridding PACS to (approximately) the same spatial sampling and equivalent monochromatic in-band measurements as IRAS and MIPS. I discuss, in detail, the procedure used in said manipulations. The results show that PACS is consistent with both IRAS and MIPS to the extent that one can discern from the host of uncertainties inherent in pixel-to-pixel comparisons. Gain factors between PACS and IRAS/MIPS are less than 17% and could potentially/simply be due to uncertainties in color-corrections or beam convolution kernels. The methodology listed here also summarizes the steps required to make pixel-to-pixel comparisons. Interested readers are urged to compare their method with the one presented here to ensure that due considerations are given to making such comparisons.

Contents

1 Introduction **3**

2 Data & Data Reduction **3**
2.1 Which MADmap map to use? . . . 3
2.2 Data reduction and map-making consideration . . . 3

3 Pixel-to-Pixel brightness comparison **4**
3.1 Conversion to surface brightness units. . . . 5
3.2 Beam Convolution . . . 5
3.2.1 PACS to IRAS . . . 5
3.2.2 PACS to Spitzer/MIPS . . . 5
3.3 Spatial Resampling/Regridding . . . 6
3.4 Region masks . . . 6
3.5 Color corrections . . . 6
3.6 Wavelength correction . . . 9
3.7 The final products . . . 9

4 Results & Discussion **9**

5 Conclusions **13**

1 Introduction

The measurement of the brightness of non point-like sources is one of the key functions of any astronomical imager such as PACS. However, surface brightness measurements are more complicated than point-source photometry because simple metrics such as aperture photometry are no longer useful. Further, unlike stars or asteroids, there are no absolute calibrators for the surface brightness (MSX calibration spheres being the exception). The best calibrated instruments for extended emission remain the COBE instruments which measured the theoretically predicted and measured microwave background radiation (see e.g. [RD1]). The IRAS full sky survey provided another opportunity to determine the absolute flux levels for the extended emission (primarily dust emission) in the mid- and far-IR wavelengths. [RD1] recalibrated the original IRAS measurements to the COBE/DIRBE experiment, thus providing absolutely calibrated all-sky images at the IRAS wavelengths . In addition, the Spitzer/MIPS 70 μm channel provides direct comparison with PACS wavelengths. In the report, we capitalize on the availability of re-calibrated IRAS (IRIS) and MIPS images to investigate the surface brightness calibration for PACS.

2 Data & Data Reduction

Table 1 lists the data used for making the comparisons reported here. The PACS data were reduced using a standard reduction script for MADmap processing (identical to, but predating, the *ipipe* script available with HIPE version 6.0). The time-lines are also calibrated using calibration derived from point source standard stars (see [RD3] & [RD4] for details). **Note: The level 1 data were further recalibrated using (as yet unpublished FM6 responsivity values)**. The FM6 responsivity values are a re-derivation of PACS calibration based on scan-map observations of flux standard stars and affects the resulting surface brightness values by up to 20%.

The level 1 data are projected to create maps using the MADmap branch of scan map pipeline. The optimal map-making algorithm used here, MADmap, is written and discussed by [RD2]. The afore-mentioned script uses pre-processing to clean the individual bolometer timelines of instrumental effects and mask the cosmic ray hits (also referred to as glitches) prior to using MADmap.

The reference fields used for comparison are from Spitzer/MIPS and IRAS images. The IRAS data are actually IRIS images as re-calibrated by [RD1] and taken from the IRSA web-site. The Galactic field used here is part of the MIPSGAL [RD5] and HiGal [RD6] survey. Spitzer/MIPS data are obtained from the MIPSGAL team (priv. comm.) and discussed by [RD5].

2.1 Which MADmap map to use?

The MADmap software produces two maps: (i) a so-called naive map in which the final map is produced by projecting (averaging together) all valid readouts for each sky pixel. There are no corrections for *1/f* drifts. The naive maps, thus, contain the striping artifacts from the *1/f* noise drifts in the final maps. (ii) The second map is the optimally extracted map from the time-lines as described by [RD2]. This map removes the *1/f* noise and creates an "optimal" solution for the projected sky values.

We chose the naive maps for this comparison. The primary motivation is the assumption in MADmap (and indeed in all map-makers) that the noise has a zero mean. Thus, averaged time-lines from the bolometers preserve the overall flux even when clear noise artifacts (e.g. striping) are present in the data at small spatial (few arc-seconds) or time scales ($\sim$100 readouts). Further, naive maps are robust to future changes in the noise filters (the so-called INVNTT files). The naive maps are also always consistently available for all MADmap reductions; Thus, if we calibrate the naive maps, then any optimally extracted map can subsequently be internally (re)calibrated to the naive maps, if necessary.

Table 1: List of Input data used for surface brightness comparison.

Field	OBSID	Filter	Size (degrees)
RCW 120	1342185553	Green	30'x30'
	1342185554	Green	30'x30'
RCW 79	1342188880	Green	30'x30'
	1342188881	Green	30'x30'
RCW 82	1342188882	Green	30'x30'
	1342188883	Green	30'x30'
L30	1342186275	Blue	2x2 degrees
	1342186276	Blue	2x2 degrees

2.2 Data reduction and map-making consideration

The PACS bolometers are calibrated on maps as opposed to time-lines. Thus, the algorithms used to create final maps from time-lines or raw readouts provide the primary inputs for the calibration process. The projection procedure, and uncertainties, is discussed extensively by [RD7]. Of relevance to this report are the following reduction steps:

- The pipeline subtracts the median value of each bolometer time-line from every single readout of that bolometer. This is necessary in order to remove pixel-to-pixel electronic offsets in the Level 1 generated signal values.
- The pipeline removes the lowest frequency drifts in the signal time lines by modeling and subtracting the signal baseline as a polynomial. [RD8] describes how the baselines are determined and removed.
- Due to the nature of iterative solution finder codes, the MADmap algorithm, furthermore, creates maps with somewhat arbitrary zero point. See ([RD2])
- The projection code used in creating maps of the flux standard stars homogenizes the optically and physically distorted individual bolometer pixels to a uniform and ideal (square) projected sky grid of pixels (see [RD4] for details). The homogenization accounts for the actual active pixel fraction. Errors in knowledge about the actual active pixel fraction do not affect the maps made from the same projection code used on flux standard stars; However, this uncertainty could potentially affect MADmap projected maps. We have tested MADmap against other projection codes and find that any error due to uncertainty in the active pixel fraction must be less than 5%.

The end result of the various time-line and baseline subtraction steps is that the zero level of the final maps is not known in PACS images and must be recovered from independent sources.

3 Pixel-to-Pixel brightness comparison

The idea here is to directly compare point-by-point surface brightness between PACS and other available independent measurements. To do this, we follow the approach adopted by [RD1] and define the comparison as:

$$I_\lambda^{\rm X} \quad = \quad G_\lambda \times I_\lambda^{\rm PACS} + B_\lambda \tag{1}$$

Where, G_λ is the gain correction factor, B_λ is the constant zero-point offset, I_λ denotes the measured monochromatic surface brightness, and the superscript on I_λ indicates the source. I use $^{\rm X}$ to mean any other independent measurements. In this report Spitzer/MIPS and IRAS data are the only ones considered.

PACS report signal values in units of Janskies per homogenized sky pixel ([RD4]) in their final maps. IRAS and MIPS on the other hand use MJy/sr as their final map units. The latter two also have beams (and hence

spatial resolutions) that are significantly broader than PACS. In addition, filter profiles and (in the case of IRAS) central wavelengths are significantly different between the two. Thus, one is required to apply careful "conversion" or manipulation steps on PACS data to ensure the accuracy of pixel-to-pixel comparison. Failure to properly apply these steps introduces systematic offsets between PACS and IRAS/MIPS that can affect both the gain factor or (less likely) the zero-point in Equation 1.

The above description should highlight that unlike total flux comparison, pixel-to-pixel type of comparisons are fraught with difficulties and it is easy to introduce a systematic gain between PACS and experiment X because many of the crucial quantities (e.g. color-correction) are either not well-known or not applied properly. Therefore, a realistic goal of these comparison should NOT be to expect 100% corroboration. Rather, we discuss the results as within or outside of the expected range determined by carefully considering both systematic (but largely unknown) errors and random errors.

I will now discuss each of the steps involved in pixel-to-pixel comparison in order of application below and highlight potential pitfalls for introducing systematic gain factors. Each operation, except color-correction, is applied to the PACS image and the reference image is left undisturbed.

3.1 Conversion to surface brightness units.

The PACS calibration scheme is designed to remove the effect of pixel-to-pixel geometry variations (see [RD4]). And, as listed in Section 2.2, the final PACS mosaics contain units of Jy per homogenized detector pixel. The size of the homogenized detector pixel is a user-defined parameter in the mapping software. For MADmap/Naivemap images used here, I chose the pixel size to be the nominal pixel sizes quoted for the PACS array: 3.2"/pixel for the short-wavelength array and 6.4"/pixel for the long-wavelength (red) array. The unit conversion values to MJy/sr are thus:

$$\text{Blue or Green}: \; 1\frac{\text{Jy}}{\text{Pixel}} = 4154.80\;\frac{\text{MJy}}{\text{SR}}$$

$$\text{Red}: \; 1\frac{\text{Jy}}{\text{Pixel}} = 1038.70\;\frac{\text{MJy}}{\text{SR}}$$

3.2 Beam Convolution

The IDL procedure *CONVOL*, provided with the ASTROLIB package, is used to perform the actual convolution. Glitches were already removed from the data and masked during the map-making process. We use the NaN and EDGE_TRUNCATE keywords in the call to *CONVOL* to account for both undefined and edge values in the data. Further details are segregated in the sections below.

3.2.1 PACS to IRAS

For IRAS reference images, we used a circular Gaussian beam as the convolution kernel to apply to PACS data. The properties of this Gaussian are taken from [RD1] in their summary and resampling to IRIS images. For the 60 μm image, the value is 4.3 arc-minutes. In fact, IRAS beams are non-circular. The sizes quoted by [RD1] for IRIS images are for equivalent circular Gaussian beam based on fitting the azimuthally averaged observed power spectra of cirrus. The averaged beam approximation of [RD1] used here will have a minor impact (less than a few percent) on the conclusions. This is because the differences in the power between circularized and "real" IRAS beams is of that order. Additionally, IRAS beams are much, much larger than PACS and small differences in either astrometry or beam sizes are diluted since the dominant power in the beam is in the central, broad Gaussian-like peak.

3.2.2 PACS to Spitzer/MIPS

The similar comparison to MIPS 70 μm filter is trickier because, unlike IRAS, the MIPS PSF is only x3 larger than PACS. Beam convolution kernels, therefore, play a very significant role. The ideal approach would be to derive a specific convolution kernel based on distorted PACS PSF and MIPS. The PACS beam is distorted in the scan direction by the on-board averaging procedure and is unique for each observation in that coverage (number of up, down, and cross- scans) determine the final shape of the PSF. These kernels will be asymmetric and will then need to be applied to individual readouts (or scan-legs at a minimum with due consideration for "turnaround" frames) before mosaicking. The ideal approach is not used here because it adds a high degree of complexity and processing overhead. Instead, as for IRAS, I derived circularized convolution kernels based on both Gaussian beams and actual MIPS beams. The difference between the two is used as a guide to roughly quantify the magnitude of error introduced by assumptions in the convolution kernels.

New Convolution Kernels

I derived convolution kernels based on the approach used by G. Aniano (Princeton, KINGFISH team). The procedure is as follows:

- First the individual MIPS and PACS PSFs are circularized. This step does introduce an error in that both PACS and MIPS beams are not symmetric. And, as discussed above, PACS asymmetries are scan-direction dependent that are difficult to deal with. However, circularization offers the least error prone approach in that it is more important to preserve the relative beam radial profile than individual assymmetric "bumps" and "wiggles" in the PSF.
- The beams are resampled and centered on to a homogeneous pixel grid.
- The MIPS beam is then "deconvolved" with the PACS beam to produce the convolution kernel. This is not a direct deconvolution but a best likelihood estimation.
- The convolution kernel is then spatially resampled to the same pixel size as the PACS maps.

Figure 1 & 2 illustrates the procedure of determining the MIPS convolution kernels. The final size of the kernels is 2.5 arc-minutes and the kernels are normalized to conserve flux during the convolution process.

3.3 Spatial Resampling/Regridding

After convolution, the PACS image are resampled to the pixel scale of the IRIS or MIPS images using the IDL procedure *HASTROM*. No astrometry offsets correction was required to re-register PACS images. Likely, this is because the astrometry error associated with both surveys is much smaller than the final sampling size (pixel size) of IRIS or MIPS images.

3.4 Region masks

Only the region containing an overlap between the scan and cross-scan observations is actually used for the flux comparison. To achieve this, I either defined a usable pixel mask, or simply ignored the non-overlap region during the mosaic creation.

3.5 Color corrections

Color correction must be applied to both PACS and the reference datasets since both report mono-chromatic equivalent brightnesses from their filter profiles. Color corrections are important because the gain factor in equation (1) has two dependencies: the calibration itself and color terms. We have used two types of fields in our analysis: Galactic Hi-Gal fields and H II regions. For both, the ideal approach is to apply the color correction to each of the astrophysical component individually. But, this is impossible since individual sources

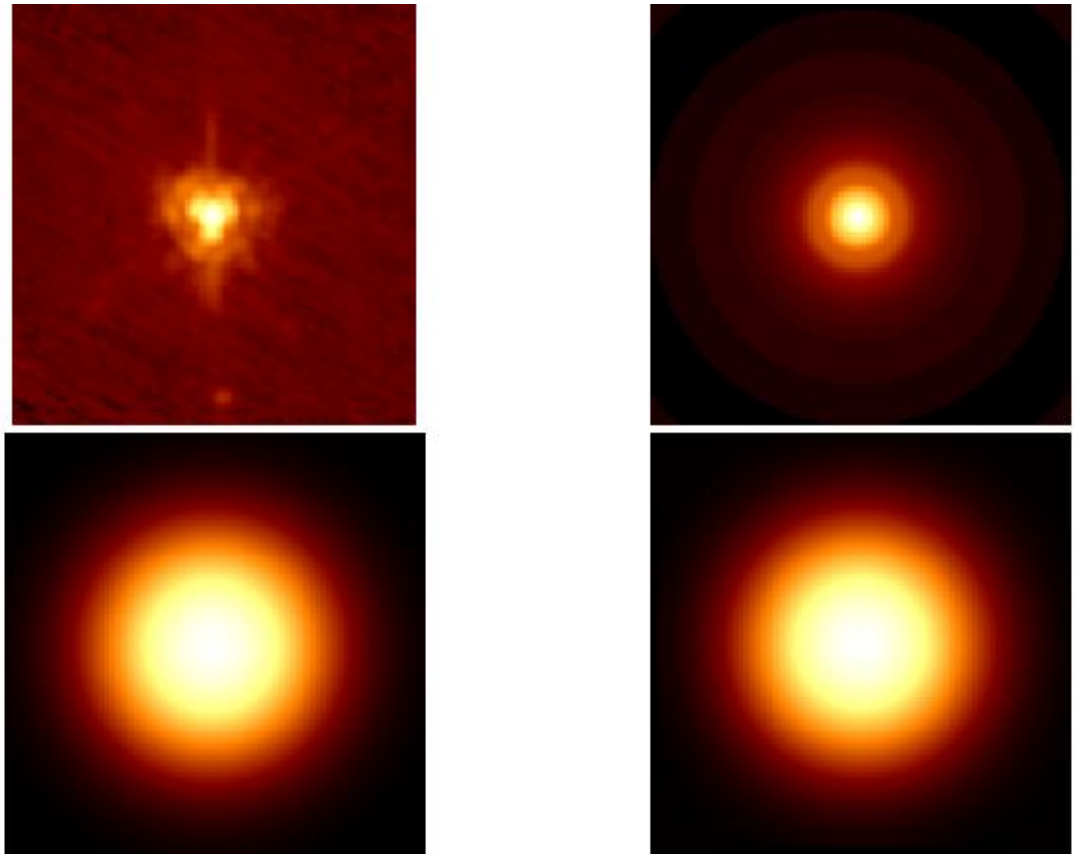

Figure 1: Beams and convolution kernels. Top left: PACS, Top Right: PACS circularized, Bottom Left: MIPS circularized, Bottom right: Convolution Kernel

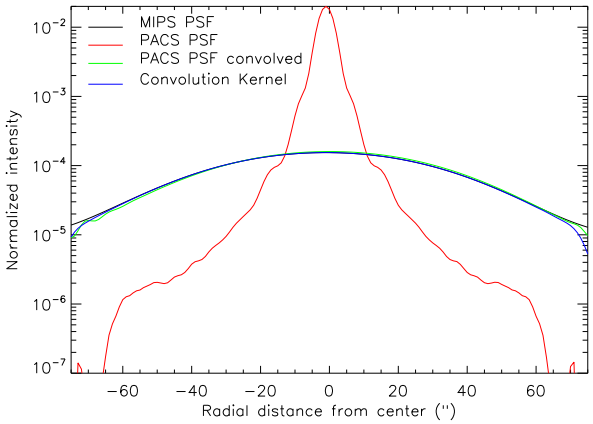

Figure 2: Radial profiles of the PSFs and convolution kernels.

Table 2: Color-corrections for the ISM.

Wavelength(s) (μm)	IRAS	MIPS	PACS	Ratio
60, 70	1.22		1.21	1.01
100	1.03		1.02	1.01
70		1.44	1.21	1.19

are blended within the beam profiles of both PACS and MIPS. As with beam convolution, a more pragmatic/realistic approach is to use an average ISM dominated color-correction and estimate the error introduced by unknown/inaccurate color-correction on the gain factors.

Figure 3 shows the expected (and normalized) emission from the ISM model with the IRAS, MIPS and PACS filter transmission profiles. The ISM spectrum itself is the model used by Spot and HSpot software. The filter profiles for IRAS are taken from the IRAS explanatory supplement and the PACS calibration files for IRAS and PACS filters, respectively. The MIPSGAL team provided the MIPS filter profiles. I derive color-corrections for the ISM in the same manner as [RD1]. The resulting values are listed in Table 2. We note that while the color-terms for the IRAS 60 and 70 μm filters are significant, the *relative* correction between the two is not. This is likely because the two filter differ most significantly in their transmission profiles at the shortest wavelengths, where the ISM emission itself is the weakest. For MIPS 70 μm the ratio of color-correction is still significant.

In the green (100 μm) band, both IRAS and PACS filters have very similar effective wavelengths as well as symmetric profiles. Such an arrangement produces very little overall color term for the ISM.

To estimate the magnitude of any systematics introduced by uncertainties in color-correction, M. Compiegne (private communication) used the DUSTEM model ([RD9]) to produce the ratio of color-correction between PACS and Spitzer/MIPS for an extreme range of Galactic conditions from coldest dust to H II regions, and for a range of small to large dust grain mixtures. His results are summarized in Figure 4. I note a variation of less than 10% between the extreme conditions used in these simulations.

3.6 Wavelength correction

One additional step is needed only for the IRAS and PACS 70 μm filter comparison. This final step is to shift the IRIS mono-chromatic brightness from 60 μm to 70 μm by applying a ratio of 60 to 70 μm flux densities in the ISM spectrum. Here, we use a single ISM spectrum (see Section 3.5) to estimate this ratio for the entire image.

3.7 The final products

Figures 5 & 6 illustrate, as an example, the evolution of the original PACS data to MIPS and IRAS spatial resolution and sampling after some of the critical steps are applied.

4 Results & Discussion

Figures 7 to 10 summarize the results from this investigation for the two filters in the PACS short wavelength (blue) array. The methodology has been discussed above.

Figure 7 shows pixel-to-pixel brightness comparison for 3 Galactic H II regions between PACS 100 μm (green filter) naivemap images and IRIS images. As discussed in Section 2.2, the zero point offset is expected to be present in these comparisons because PACS data processing must remove local backgrounds. The average gain factor is 0.83 and the three regions agree to within 10% of the average value. The gain factors are derived by fitting a line to the observed distribution taking care to ignore the points below 10 MJy/sr in the fitting.

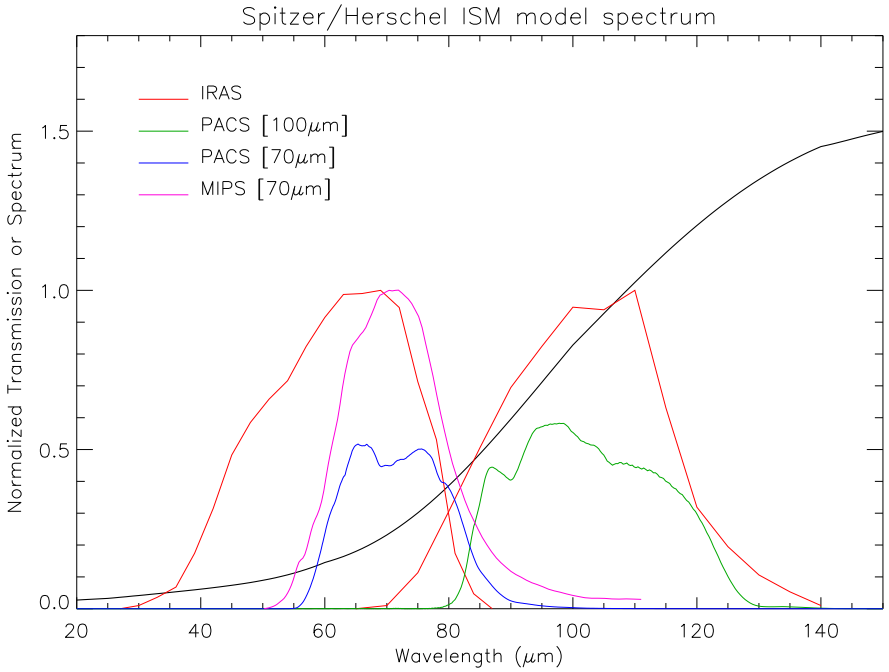

Figure 3: The interstellar medium spectrum (black line) from the Spitzer/Herschel background model overlayed with the IRAS, MIPS and PACS filter profiles. The longer wavelength 100 μm filters are symmetric and roughly equivalent. The bluer 60 and 70 μm filters are not; however, the ism spectrum shows little or no emission where the differences between the filters are largest.

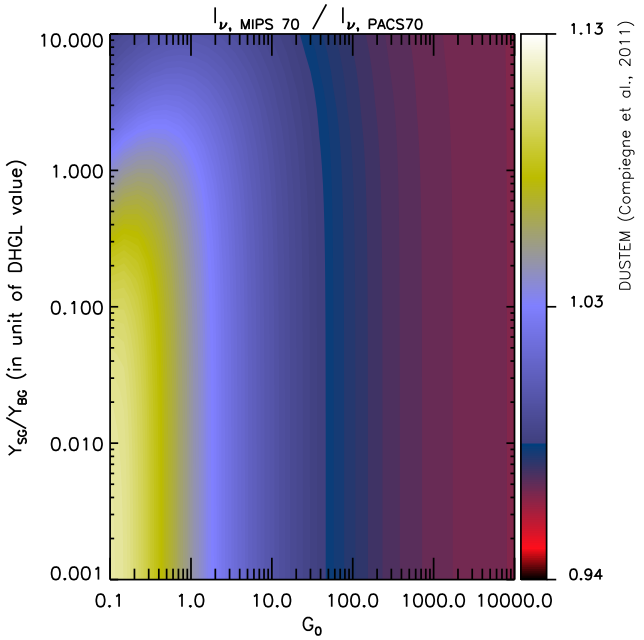

Figure 4: Color-correction variation between PACS and MIPS filters as estimated by the ratio of simulated PACS to MIPS brightnesses. The color-bar indicates the magnitude of the ratio. The x-axis shows the range of ISM conditions considered in this simulation. The y-axis shows the range of dust mixture considered. Less than 10% variation exists between the extremeties.

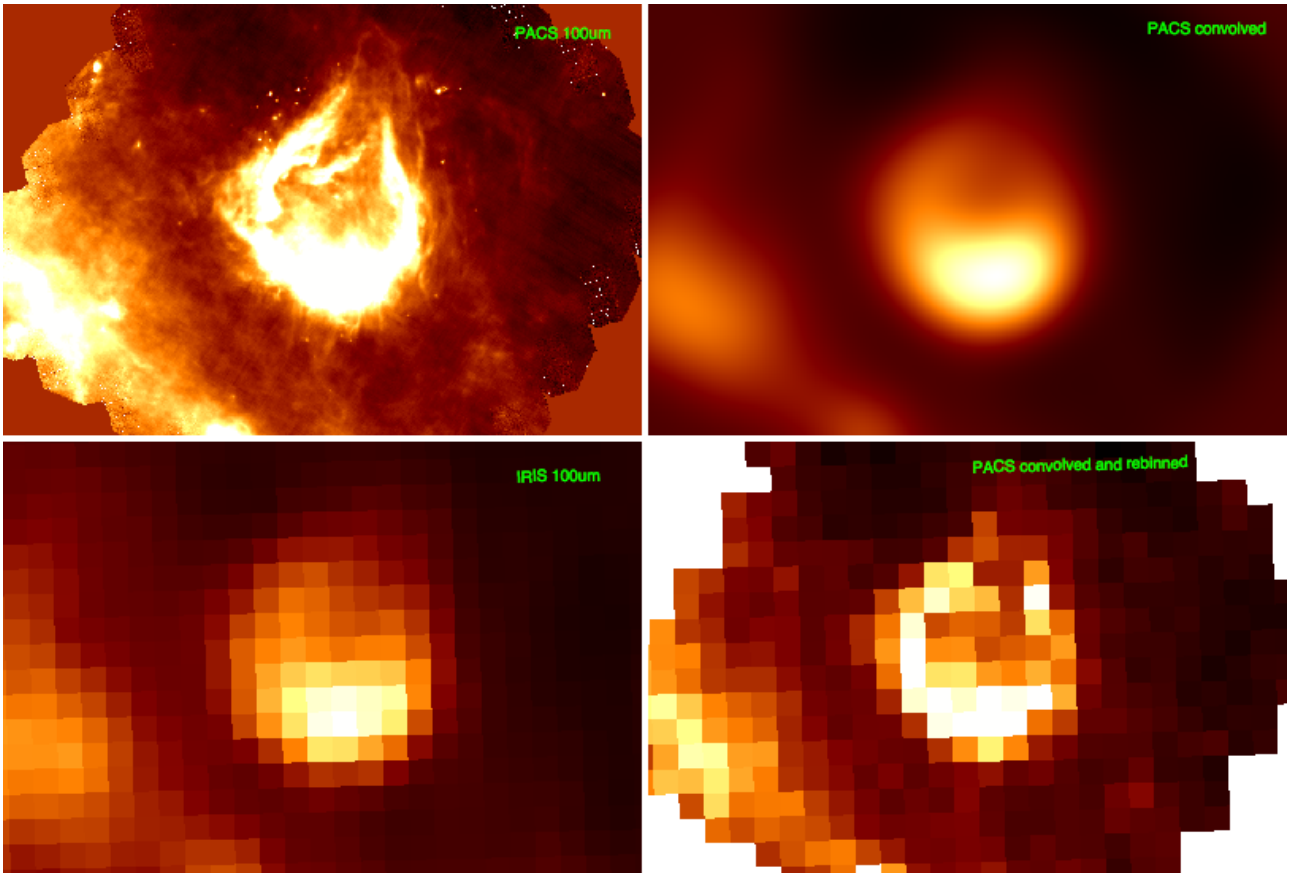

Figure 5: The PACS observation of the field RCW 120 convolved and resampled to IRIS spatial resolution. Clockwise from top left are the original PACS "naive" map, the convolved PACS image, the convolved and resampled PACS image. And, for comparison, the bottom left panel shows the IRIS image of the same region.

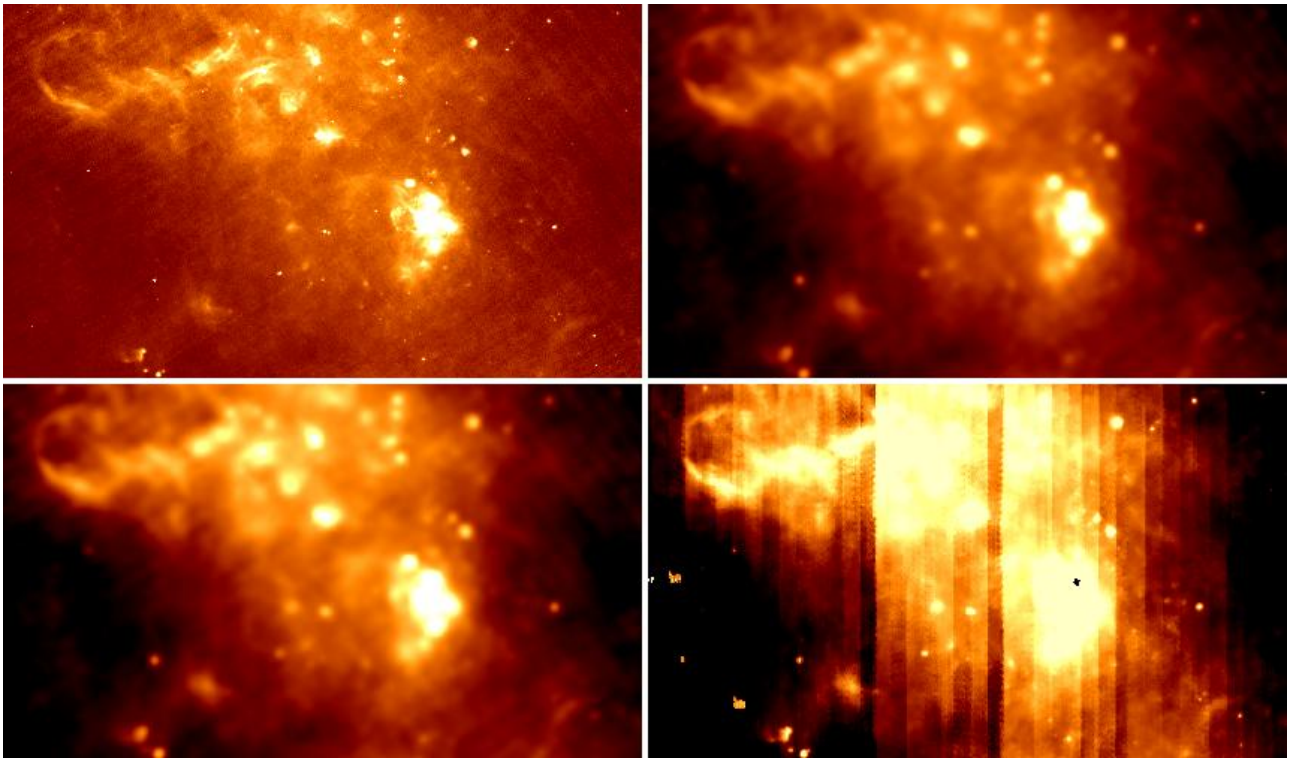

Figure 6: Same as Figure 5 but for the L30 Hi-Gal field and MIPSGAL images. Here the bottom right panel shows the MIPSGAL image. Note the presence of strong reduction artifacts (offsetting stripes) in the MIPSGAL image.

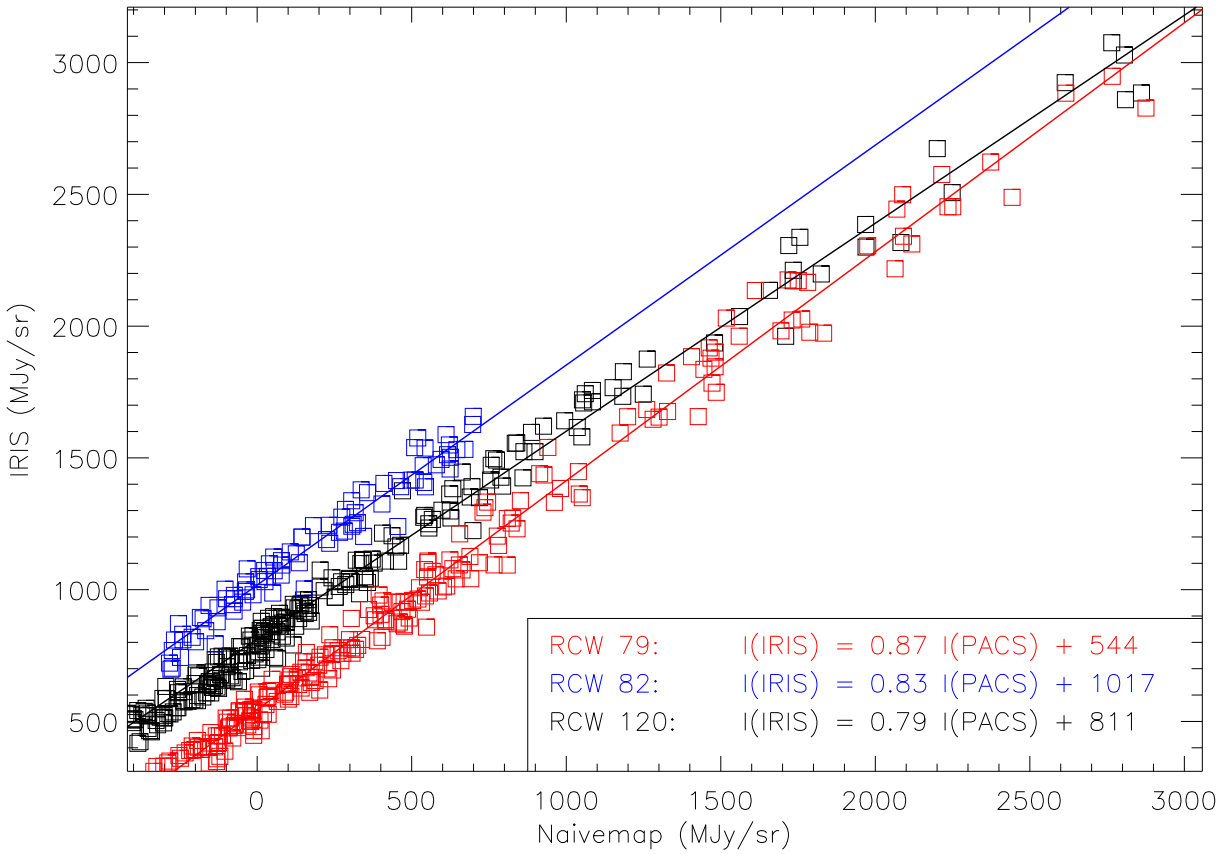

Figure 7: The IRIS surface brightness plotted against the PACS "naive map" surface brightness measurements. The red, black and blue symbols and lines show the results for RCW 79, 120 and 82, respectively. The solid lines show the best-fit linear model. The measured gain factors for all best-fit lines are shown in the inset legend box.

Brightness value below 10MJy/sr suffer from noise introduced by the so-called $1/f$ noise of the bolometers in the naivemaps.

Similarly, Figure 8 shows pixel-to-pixel brightness comparison between PACS and MIPS for the 70 μm filter. The results are shown both for a Gaussian convolution kernels as well as the new kernel discussed in Section 3.2.2. The newer kernels shows less overall scatter but changes the gain value by less than 5%. The change is; however, in the direction of better agreement between PACS and MIPS. However, regardless of this small improvement, the comparison is dominated by artifacts in the MIPS image (offset differences between scan lines) and to a lesser degree by the $1/f$ noise in PACS image.

A more apt comparison of the pixel-to-pixel fluxes between PACS and MIPS actually must come from both down sampled to spatial pixels equivalent to IRIS images. This is because the MIPSGAL team, being aware of systematic offset artifacts introduced by, among others, pcal flashes calibrated MIPSGAL tiles with IRIS images. Thus, MIPSGAL calibration in only truly ensured on spatial scales as large as the IRIS beam. Figure 9 shows the results when both PACS and MIPS are instead resampled to the pixel sizes of IRIS images. The observed scatter seen in Figure 8 is now significantly decreased, and gain factor estimated from the best-fit line is identical to the one derived for the H II regions (above).

Figure 10 shows the comparison between PACS and the IRIS image of the same HiGal field using the procedures discussed above. The best-fit correlation line has a slope, gain, of 1.12, higher than ones reported so far.

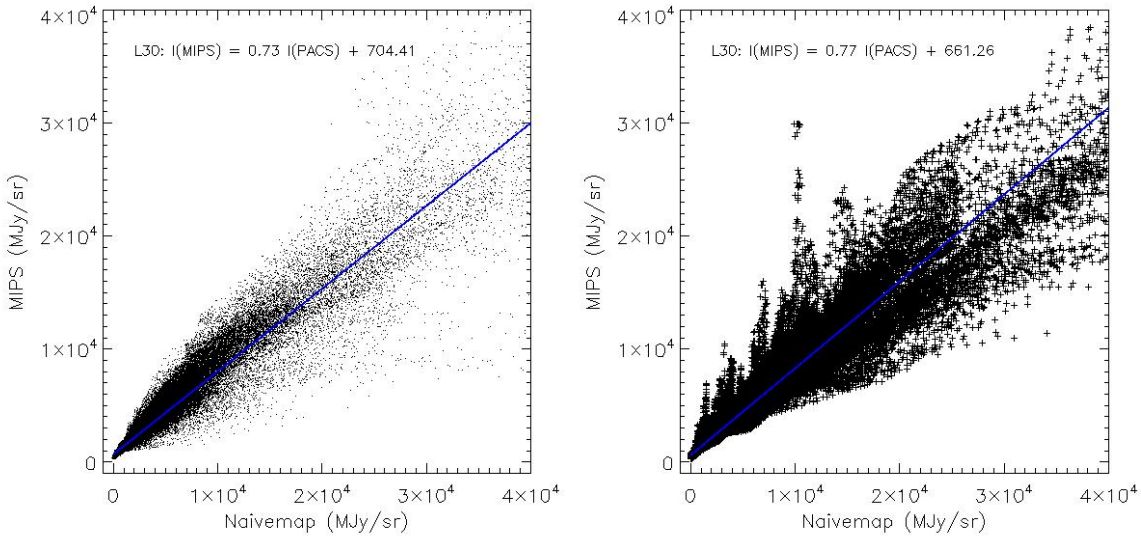

(a) Gaussian Kernel

(b) Kernel2

Figure 8: Direct pixel-to-pixel brightness comparison between MIPS and PACS using a Gaussian kernel (left) and one derived from MIPS and PACS beams (right).

Table 3: Gain factors and zero-point offsets determined in this investigation.

PACS Fillter	λ (μm)	Field	G_λ (MJy/sr)	B_λ	Reference
Green	100	RCW 120	0.79	811	IRAS
Green	100	RCW 79	0.87	544	IRAS
Green	100	RCW 82	0.83	1017	IRAS
Blue	70	Galactic Field	0.83	616	Spitzer/MIPS
Blue	70	Galactic Field	1.12	164	IRAS

Table 3 summarizes the gain and zero-point offsets values from this investigation. The observed gain between PACS and IRAS/MIPS is less than 20%. **These values should NOT be used to apply any correction to PACS data.** At this level, differences between PACS and IRAS/MIPS can easily be explained as combination of errors in convolution kernel (see Section 3.2), color correction (see Section 3.5) and measurement errors and uncleaned artifacts in the data. These factors limit the accuracy of the comparison performed here and to the extent that it can be determined, PACS surface brightness values are consistent with IRAS and MIPS.

5 Conclusions

For the PACS blue channel, the primary results of this investigation are: (i) that PACS calibration scheme derived from point source photometry is applicable and correct for extended sources. (ii) Within the known limitation of this investigation, there is no justification for applying gain corrections to PACS images. And, (iii) comparison of surface brightness values between two independent experiments requires careful manipulation of data and requires due consideration to be paid for each step. The manipulation steps relevant to said comparisons have been described in this report and should provide a reference for readers interested in carrying out similar comparisons.

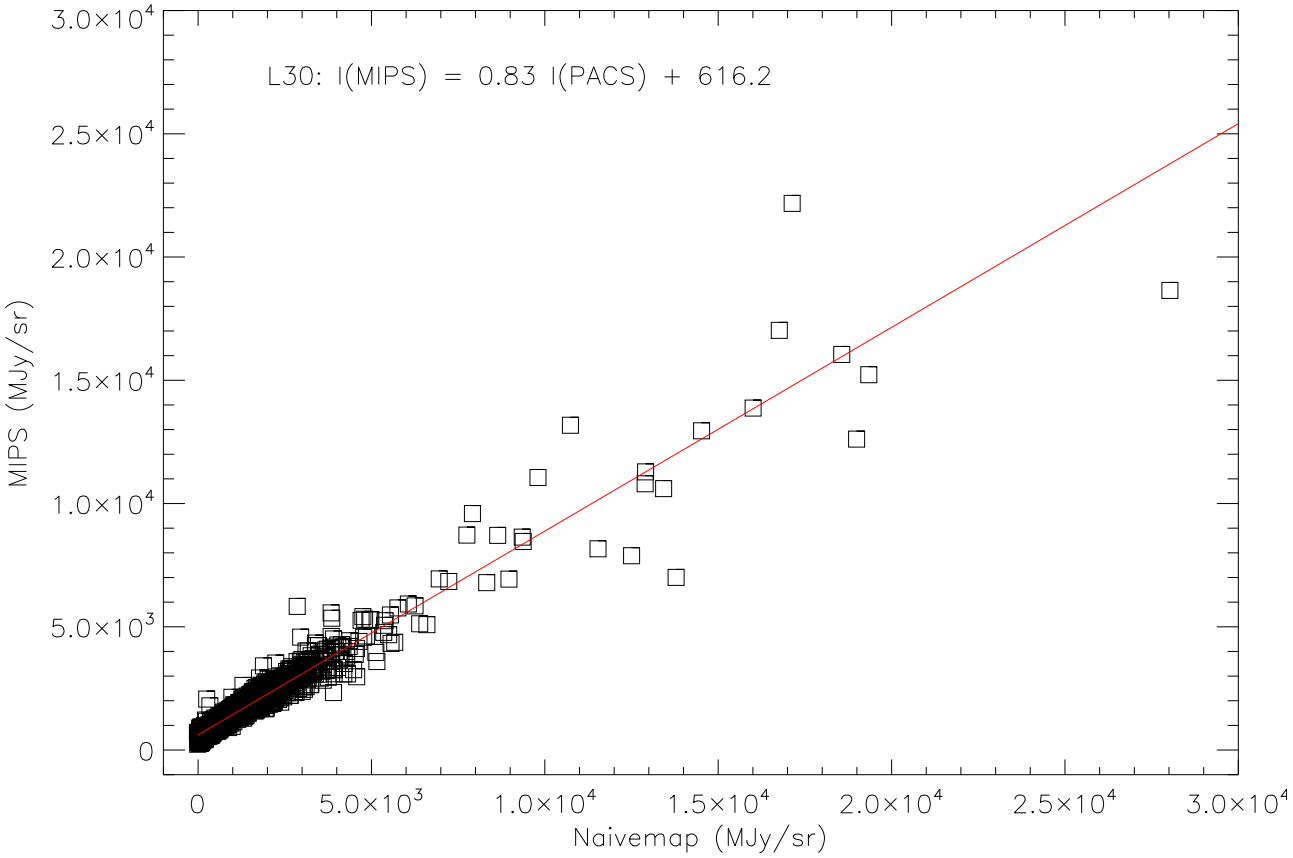

Figure 9: Direct pixel-by-pixel comparison between MIPS and PACS images using new convolution kernels at the resolution of IRIS maps.

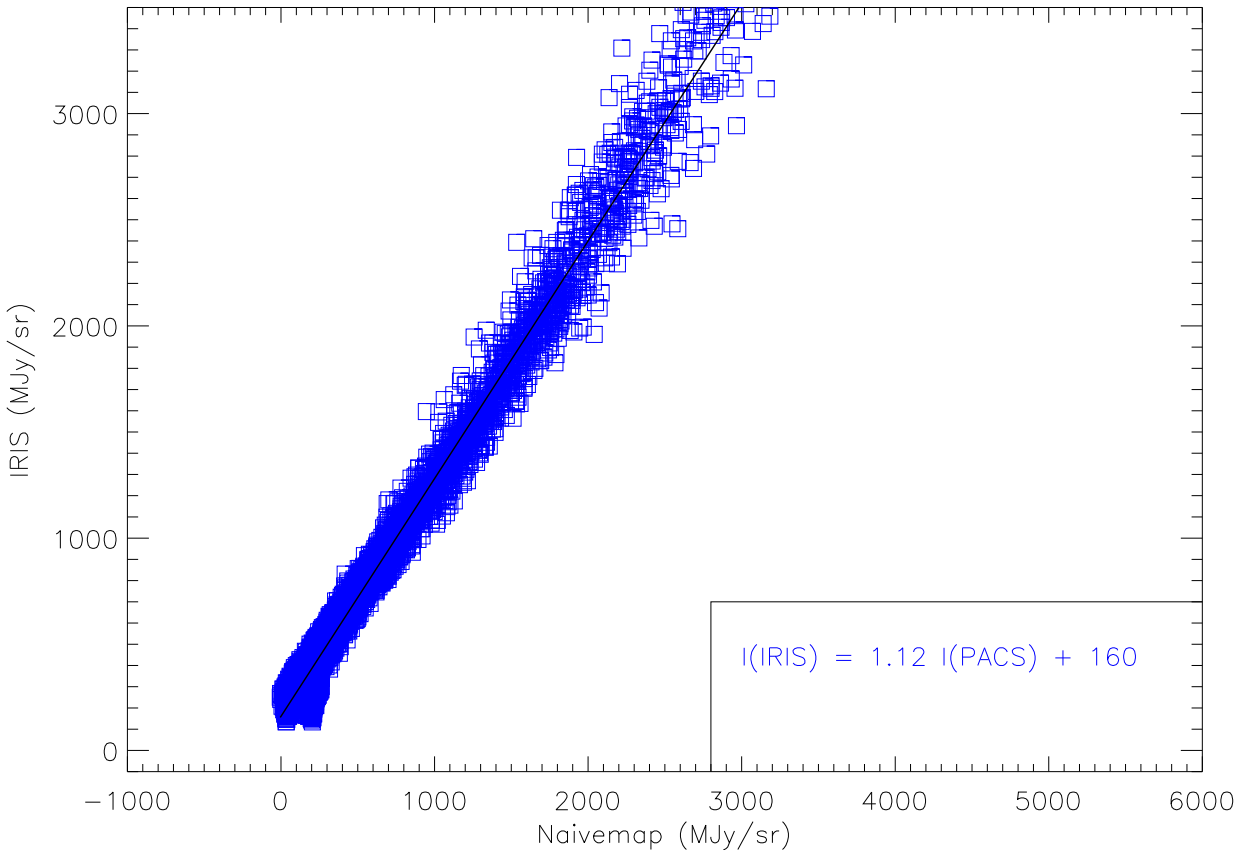

Figure 10: Direct pixel-by-pixel comparison between IRIS and PACS images.

Future versions of this report will extend the analysis to additional PACS fields.

References

[RD1] Meville-Deschenes, M.-A. & Lagache, G. (2005), ApJS, 157, 302

[RD2] Catalupo et al. (2009) http://arxiv.org/pdf/0906.1775

[RD3] Müeller, T., PICC-ME-TN-036 "PACS Scan map release note" Version 2.0

[RD4] Sauvage, M., SAp-PACS-MS-0717-11 "Projection Math" Version 1.0

[RD5] Carey et al. (2009) PASP, 121, 76

[RD6] Molinari et al. (2010), PASP, 122, 314

[RD7] Sauvage, M., SAp-PACS-MS-0718-11 "Experiments in photometric measurements of extended sources." Version D0.1

[RD8] The PACS data reduction guide, chapter 7

[RD9] Compiégne et al. (2011) A&A, 525, 103